AFRL-RX-TY-TR-2011-0030

THEORETICAL SOLUTION FOR TEMPERATURE PROFILE IN MULTI-LAYERED PAVEMENT SYSTEMS SUBJECTED TO TRANSIENT THERMAL LOADS

Jeffery R. Roesler and Dong Wang

Department of Civil and Environmental Engineering
University of Illinois at Urbana-Champaign
901 West Illinois Street
Urbana, IL 61801

Contract No. FA4819-10-C-0008

January 2011

AIR FORCE RESEARCH LABORATORY
MATERIALS AND MANUFACTURING DIRECTORATE

■ **Air Force Materiel Command** ■ **United States Air Force** ■ **Tyndall Air Force Base, FL 32403-5323**

DISCLAIMER

Reference herein to any specific commercial product, process, or service by trade name, trademark, manufacturer, or otherwise does not constitute or imply its endorsement, recommendation, or approval by the United States Air Force. The views and opinions of authors expressed herein do not necessarily state or reflect those of the United States Air Force.

This report was prepared as an account of work sponsored by the United States Air Force. Neither the United States Air Force, nor any of its employees, makes any warranty, expressed or implied, or assumes any legal liability or responsibility for the accuracy, completeness, or usefulness of any information, apparatus, product, or process disclosed, or represents that its use would not infringe privately owned rights.

This report does not conform to the current guidance by the United States Air Force Research Laboratory. It is being submitted in its original format, as generated by the authors of the report.

NOTICE AND SIGNATURE PAGE

Using Government drawings, specifications, or other data included in this document for any purpose other than Government procurement does not in any way obligate the U.S. Government. The fact that the Government formulated or supplied the drawings, specifications, or other data does not license the holder or any other person or corporation; or convey any rights or permission to manufacture, use, or sell any patented invention that may relate to them.

This report was cleared for public release by the 88th Air Base Wing Public Affairs Office at Wright Patterson Air Force Base, Ohio and is available to the general public, including foreign nationals. Copies may be obtained from the Defense Technical Information Center (DTIC) (http://www.dtic.mil).

AFRL-RX-TY-TR-2011-0030 HAS BEEN REVIEWED AND IS APPROVED FOR PUBLICATION IN ACCORDANCE WITH ASSIGNED DISTRIBUTION STATEMENT.

CUBILLOS FONSECA.ANGELICA.NMN .1258842541
Digitally signed by CUBILLOS FONSECA.ANGELICA.NMN.1258842541
DN: c=US, o=U.S. Government, ou=DoD, ou=PKI, ou=USAF, cn=CUBILLOS FONSECA.ANGELICA.NMN.1258842541
Date: 2011.04.26 10:22:58 -05'00'

ANGELICA CUBILLOS, 2nd Lt, USAF
Work Unit Manager

RICHLIN.DEBRA.L .1034494149
Digitally signed by RICHLIN.DEBRA.L.1034494149
DN: c=US, o=U.S. Government, ou=DoD, ou=PKI, ou=USAF, cn=RICHLIN.DEBRA.L.1034494149
Date: 2011.07.28 13:18:47 -05'00'

DEBRA L. RICHLIN, DR-III
Acting Chief, Airbase Engineering Development Branch

RHODES.ALBERT .N.III.1175488622
Digitally signed by RHODES.ALBERT.N.III.1175488622
DN: c=US, o=U.S. Government, ou=DoD, ou=PKI, ou=USAF, cn=RHODES.ALBERT.N.III.1175488622
Date: 2011.07.29 10:24:53 -05'00'

ALBERT N. RHODES, PhD
Chief, Airbase Technologies Division

This report is published in the interest of scientific and technical information exchange, and its publication does not constitute the Government's approval or disapproval of its ideas or findings.

REPORT DOCUMENTATION PAGE

Form Approved
OMB No. 0704-0188

PLEASE DO NOT RETURN YOUR FORM TO THE ABOVE ADDRESS.

1. REPORT DATE *(DD-MM-YYYY)*	2. REPORT TYPE	3. DATES COVERED *(From - To)*
01-FEB-2011	Final Technical Report	01-FEB-2010 -- 31-JAN-2011

4. TITLE AND SUBTITLE

Theoretical Solution for Temperature Profile in Multi-layered Pavement Systems Subjected to Transient Thermal Loads

5a. CONTRACT NUMBER

FA4819-10-C-0008

5b. GRANT NUMBER

5c. PROGRAM ELEMENT NUMBER

0909999F

6. AUTHOR(S)

Roesler, Jeffery R.; Wang, Dong

5d. PROJECT NUMBER

4915

5e. TASK NUMBER

D0

5f. WORK UNIT NUMBER

QD101003

7. PERFORMING ORGANIZATION NAME(S) AND ADDRESS(ES)

Department of Civil and Environmental Engineering
University of Illinois at Urbana-Champaign
901 West Illinois Street
Urbana, IL 61801

8. PERFORMING ORGANIZATION REPORT NUMBER

9. SPONSORING/MONITORING AGENCY NAME(S) AND ADDRESS(ES)

Air Force Research Laboratory
Materials and Manufacturing Directorate
Airbase Technologies Division
139 Barnes Drive, Suite 2
Tyndall Air Force Base, FL 32403-5323

10. SPONSOR/MONITOR'S ACRONYM(S)

AFRL/RXQEM

11. SPONSOR/MONITOR'S REPORT NUMBER(S)

AFRL-RX-TY-TR-2011-0030

12. DISTRIBUTION/AVAILABILITY STATEMENT

Distribution Statement A: Approved for public release; distribution unlimited.

13. SUPPLEMENTARY NOTES

Ref Public Affairs Case # 88ABW-2011-4206, 29 July 2011. Document contains color images.

14. ABSTRACT

This technical report focuses on developing easily implemented analytical solutions to predict rapidly varying temperature profiles in concrete pavements subjected to transient thermal loadings generated by vertical take-off aircraft engines. The general closed-form solution for the one-dimensional (1-D) temperature profile in a homogeneous half-space with specified pavement surface temperatures is well known; efficient numerical algorithms to accurately resolve the integrals involved in the general solution are identified through literature review and recommended based on numerical experiments in this report. 1-D analytical solutions for temperature fields in a two-layered pavement system using Laplace transforms are proposed for two different surface boundary conditions, i.e., specified transient surface temperature and mixed boundary condition involving heat flux emanating from the aircraft engine. Furthermore, two-dimensional (2-D) axisymmetric temperature field in a homogeneous half-space subjected to transient thermal loading was solved under the specified surface temperature condition. Two solution methods were introduced: one based on the Hankel transforms and the method of separation of variables; another based on the Hankel and Laplace transforms. Numerical experiments suggest that the combined results based on those two methods give reasonable approximation to the rapidly varying temperature profile.

15. SUBJECT TERMS

multi-layer pavement, temperature profile, 2D temperature model, Hankel transforms, Laplace transforms, thermal loads.

16. SECURITY CLASSIFICATION OF:			17. LIMITATION OF ABSTRACT	18. NUMBER OF PAGES	19a. NAME OF RESPONSIBLE PERSON
a. REPORT	b. ABSTRACT	c. THIS PAGE			Angelica Cubillos
U	U	U	UU	56	19b. TELEPHONE NUMBER *(Include area code)*

Reset

Standard Form 298 (Rev. 8/98)
Prescribed by ANSI Std. Z39.18

TABLE OF CONTENTS

List of Tables

List of Figures

ACKNOWLEDGEMENTS

This technical report is based upon research work funded by the Air Force Research Laboratory under contract No. FA4819-10-C-0008. Any opinions, findings and conclusions or recommendations expressed in this report are those of the authors and do not necessarily reflect the views of the Air Force Research Laboratory.

Chapter 1

INTRODUCTION

1.1 Motivation

New-generation military aircraft are being developed to take off and land vertically, resulting in large thermal loads on the pavement surface. These Fast transient thermal loads produce a rapidly varying temperature profile both radially and through the slab. These repeated thermal loads can lead to premature deterioration of the airfield pavement structure. Ju and Zhang[1,2] give a detailed account on this issue. Traditional paving materials such as concrete and asphalt concrete will not have the same longevity under this condition of repeated thermal.[1–6] Accurately predicting this transient high-temperature profile is crucial and a prerequisite to further determining the thermal stress fields in the material design of this new type of airfield pavement application.

Different approaches can be applied to predict temperature fields in multi-layered pavement systems under climatic conditions, such as statistics-based models, numerical approaches, and analytical methods. Wang, Roesler, and Guo[7] present an overview of these various approaches. To estimate rapidly changing temperature profiles in concrete pavements subjected to fast transient thermal loads, numerical or analytical approach is appropriate. A numerical approach—specifically, an explicit finite difference method—was employed to predict two-dimensional (2-D) axisymmetric transient high temperature field in Ju and Zhang.[2] The main advantage of this method is that it can easily handle temperature-dependent thermal properties of concrete, such as density, specific heat, and thermal conductivity. However, an extremely small temporal step size, which is highly dependent on the spatial step-size, must be chosen to ensure computational stabilities and hence this approach is generally more time-consuming. In view of the facts that the thermal properties of concrete change slowly when the temperature increases,[2] and the huge amounts of heat exhausted from aircraft engines is the dominant driving force for this problem, a rapid analytical solution can be

pursued by assuming that thermal properties of each layer of material in pavements are constant.

The primary objective of this study is to develop easily implemented analytical solutions for predicting the rapidly varying pavement temperature profile under fast transient thermal loads. To meet different needs for acquiring temperature profile information, one-dimensional (1-D) and 2-D axisymmetric temperature fields will be considered. Time-dependent temperature profiles change only with depth in the 1-D case, and the profiles change both vertically and radially(horizontally) in the 2-D axisymmetric case. The main advantage of these analytical solutions is that they lay the foundation for further investigating the 1-D and 2-D axisymmetric thermal stress fields in concrete pavements based on analytical approaches.

1.2 Overview

The overview of this report is as follows:

In Chapter 2, 1-D temperature fields in homogeneous half-space subjected to fast, transient, thermal loadings is investigated first. The general closed-form solution for this initial-boundary problem is identified through literature review. Efficient Gaussian-type quadrature formulas developed by Steen et al. are tested and recommended to numerically resolve the general solution. This is followed by the study of 1-D temperature fields in two-layered pavement systems subjected to high-temperature transient thermal loadings. Two types of solutions are derived based on two different boundary conditions, namely, specified pavement surface temperature history, and specified heat flux intensity from aircraft engines, respectively. The main mathematical tools employed in deriving analytical solutions in these cases are Laplace integral transforms (LT) and numerical Laplace inversion. Some model calculations are performed to demonstrate the derived analytical solutions. This chapter concludes with some sensitivity studies that investigate effects of material thermal properties and thickness of the first layer on temperature profile in a two-layered pavement system.

In Chapter 3, a 2-D axisymmetric temperature field in homogeneous half-space with spec-

ified surface temperatures due to transient thermal loads is studied. Analytical solutions are derived respectively using two different methods: one based on separation of variables (SV) and HT while the other is based on LT and HT. Numerical results are obtained using the derived solutions and a model pavement surface temperature history extracted from Dr. Zhang's doctoral dissertation,[8] suggesting that a combined result based on these two different analytical solutions will give a reasonable approximation of the pavement temperature profile.

In Chapter 4, a summary of this technical report is presented.

Chapter 2

1-D TEMPERATURE FIELD IN PAVEMENTS

In this chapter, 1-D rapidly varying temperature profiles in pavements subjected to fast, transient thermal loadings is investigated. In Section 2.1, an analytical solution for such temperature profiles in a homogeneous half-space is presented. Analytical solutions for temperature profile in two-layered pavement systems are systematically studied using LT and numerical Laplace inversions in Section 2.2.

2.1 1-D Temperature Field in Homogeneous Half-Space Subjected to Fast, Transient Thermal Loadings

2.1.1 Specified Pavement Surface Temperature

The governing equation for this heat conduction problem without an internal heat source/sink is the classic 1-D heat equation

$$\frac{\partial T}{\partial t} = \alpha \frac{\partial^2 T}{\partial z^2} \qquad \text{for} \quad 0 < z < \infty \quad \text{and} \quad t > 0 \tag{2.1}$$

where α = thermal diffusivity of material (m^2/h).

One way to consider rapidly transient thermal loadings, e.g., energy projected from vertical-take-off/landing aircraft with fast heating rate (say, 500 °C/min. as used in Ju and Zhang[1]), is to use measured transient surface temperatures $F(t)$ (if available) in the area where the temperature is the highest. Mathematically, the following initial boundary value problem needs to be solved

$$\begin{aligned} \frac{\partial T}{\partial t}(z,t) &= \alpha \frac{\partial^2 T}{\partial z^2}(z,t) \qquad 0 < z < \infty \quad \text{and} \quad 0 < t < \infty \\ T(0,t) &= F(t) \qquad \text{for} \quad z = 0 \\ T(z,0) &= G(z) \qquad \text{for} \quad t = 0 \end{aligned} \tag{2.2}$$

The analytical solution for the above initial boundary value problem (Equation 2.2) can be obtained using the method of odd extension discussed in Section 3.1 in Strauss,[9] or by summing up solutions of two simpler initial-boundary-value problems outlined on page 64 in Carslaw and Jaeger.[10] The complete solution of Equation 2.2 is

$$\begin{aligned} T(z,t) &= \frac{1}{\sqrt{4\pi\alpha t}} \int_0^\infty \left[e^{-\frac{(z-y)^2}{4\alpha t}} - e^{-\frac{(z+y)^2}{4\alpha t}} \right] G(y) dy \\ &\quad + \frac{2}{\sqrt{\pi}} \int_{\frac{z}{\sqrt{4\alpha t}}}^\infty F\left(t - \frac{z^2}{4\alpha y^2} \right) e^{-y^2} dy \end{aligned} \tag{2.3}$$

provided the improper integrals in Equation (2.3) converge.

In Ju and Zhang,[1] $F(t)$ and $G(z)$ take the following forms

$$\begin{aligned} F(t) &= T_s(t) \\ &= 285 + 49.5 \ln(t + 0.00554) \end{aligned} \tag{2.4}$$

$$\begin{aligned} G(z) &= T_0 \\ &= 25 \end{aligned} \tag{2.5}$$

where t in Equation (2.4) is measured in seconds, and T_0 in Celsius degrees in Equation (2.5).

Substituting Eqs. (2.4) and (2.5) into Equation (2.3) gives

$$T(z,t) = \frac{2}{\sqrt{\pi}} \int_{\frac{z}{\sqrt{4\alpha t}}}^\infty T_s\left(t - \frac{z^2}{4\alpha y^2} \right) e^{-y^2} dy + \frac{2}{\sqrt{\pi}} T_0 \int_0^{\frac{z}{\sqrt{4\alpha t}}} e^{-y^2} dy \tag{2.6}$$

which is in agreement with Equation (5) in Ju and Zhang.[1]

It is noted that for arbitrary $z > 0$ and $t > 0$, the improper integral in Equation (2.6) can be shown to converge to a finite value by using the Lebesgue's dominated convergence theorem from real analysis. The time-dependent surface temperature described by Equation

(2.4) is plotted in Figure 2.1.

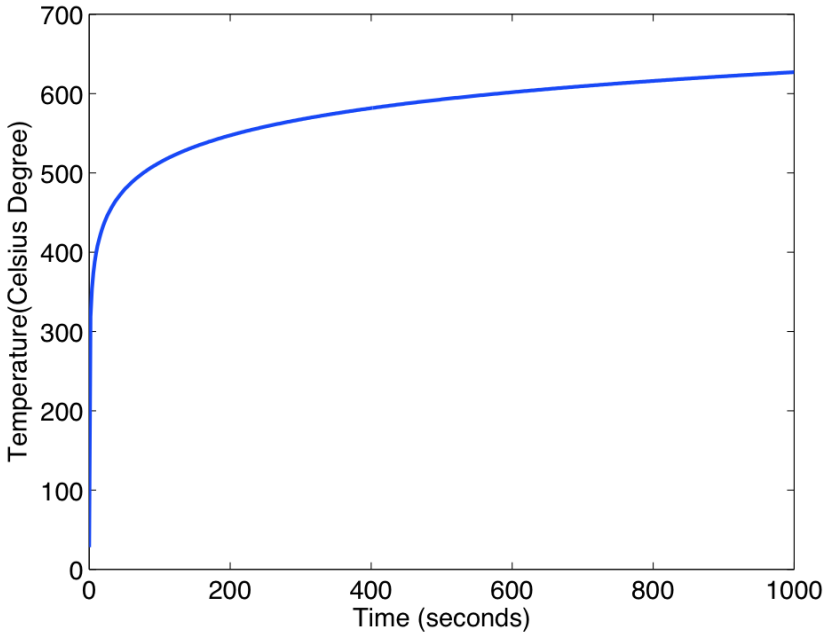

Figure 2.1: **Time-dependent Surface Temperature Due to Transient High-temperature Loadings**

Due to the complexities of integrands in the integrals in Equation (2.6), the closed-form solution of integrals in Equation (2.6) is hard to derive. Thus a numerical approximation to Equation (2.6) is employed in this study.

Steen et al.[11] developed efficient Gaussian-type integration formulas to approximate integrals of the forms

$$\int_0^\infty e^{-x^2} f(x)dx \qquad \text{and} \qquad \int_0^1 e^{-x^2} f(x)dx,$$

and their formulas are given as follows

$$\int_0^\infty e^{-x^2} f(x)dx \approx \sum_{k=1}^{N} w_k f(x_k) \tag{2.7}$$

$$\int_0^1 e^{-x^2} f(x)dx \approx \sum_{k=1}^{M} w_k f(x_k) \tag{2.8}$$

where $N \in \{k \text{ is a positive integer} : 2 \leq k \leq 15\}$; $M \in \{k \text{ is a positive integer} : 2 \leq k \leq 10\}$; weights w_k and abscissae $x_k, k = 1, 2, \ldots, N$ or M are listed in Steen et al.[11]

To apply Equations (2.7) and (2.8), the integrals in Equation (2.6) have to be transformed into the standard integral form $\int_0^\infty e^{-x^2} f(x)dx$ or $\int_0^1 e^{-x^2} f(x)dx$. This can be easily achieved using a change of variables as follows:

Let $\eta = \frac{z}{\sqrt{4\alpha t}}$ and $y = \eta + \xi$; then the improper integral in Equation (2.6) becomes

$$\int_\eta^\infty T_s\left(t - \frac{z^2}{4\alpha y^2}\right) e^{-y^2} dy = \int_0^\infty e^{-\xi^2} e^{-\eta(\eta+2\xi)} T_s\left(t - \frac{z^2}{4\alpha(\eta+\xi)^2}\right) d\xi \tag{2.9}$$

on the other hand, if we let $y = \eta\xi$, the definite integral in Equation (2.6) becomes

$$\int_0^\eta e^{-y^2} dy = \eta \int_0^1 e^{-\xi^2} e^{(1-\eta^2)\xi^2} d\xi \tag{2.10}$$

For fixed $z > 0, t > 0$, the temperature $T(z,t)$ can be approximated by applying Steen et al.'s[11] integral formulas to Equation (2.6). To investigate the effect of the concrete diffusivity coefficient α on the temperature profile, $\alpha = 1.3$ mm^2/s and $\alpha = 1.0$ mm^2/s used by Ju and Zhang[1] are adopted in this study, and $N = 15, M = 10$ are employed in Steen et al's[11] integral formulas. For the sake of completeness Tables 2.1 and 2.2 list the weights w_k and abscissae x_k used in Eqs. (2.7) and (2.8), respectively.

Figure 2.2 plots effects of concrete diffusivity coefficient α on concrete pavement temperature profile at $t = 10$ s and $t = 600$ s due to transient high-temperature loadings. Figure 2.3 presents effects of the concrete diffusivity coefficient α on transient temperature values at

Table 2.1: **Weights and Abscissae Used in Equation (2.7),** $N = 15^{11}$

k	w_k	x_k
1	0.055443366310234	0.02168694746755
2	0.124027738987730	0.11268422034777
3	0.175290943892075	0.27049267142189
4	0.191488340747342	0.48690237038193
5	0.163473797144070	0.75304368307297
6	0.105937637278492	1.06093100362236
7	0.050027021153453	1.40425495820363
8	0.016442969005267	1.77864637941183
9	0.003573204214283	2.18170813144494
10	4.82896509305201e-04	2.61306084533352
11	3.74908650266318e-05	3.07461811380851
12	1.49368411589636e-06	3.57140815113714
13	2.55270496934465e-08	4.11373608977209
14	1.34217679136316e-10	4.72351306243148
15	9.56227446736465e-14	5.46048893578335

Table 2.2: **Weights and Abscissae Used in Equation (2.8),** $M = 10^{11}$

k	w_k	x_k
1	0.032531969510180	0.012737849971374
2	0.072483896403744	0.065802327974393
3	0.104004662155270	0.156155783059660
4	0.121594475562980	0.275890718366863
5	0.122093608318116	0.414966322218475
6	0.107195747923389	0.562009142193357
7	0.083077989029486	0.704832804690269
8	0.056928598840185	0.830893869740303
9	0.033398291993499	0.928057569743495
10	0.013514893075575	0.985992766817013

$z = 1$ mm and $z = 20$ mm at different times. These results are consistent with the graphical solutions presented by Ju and Zhang.[1]

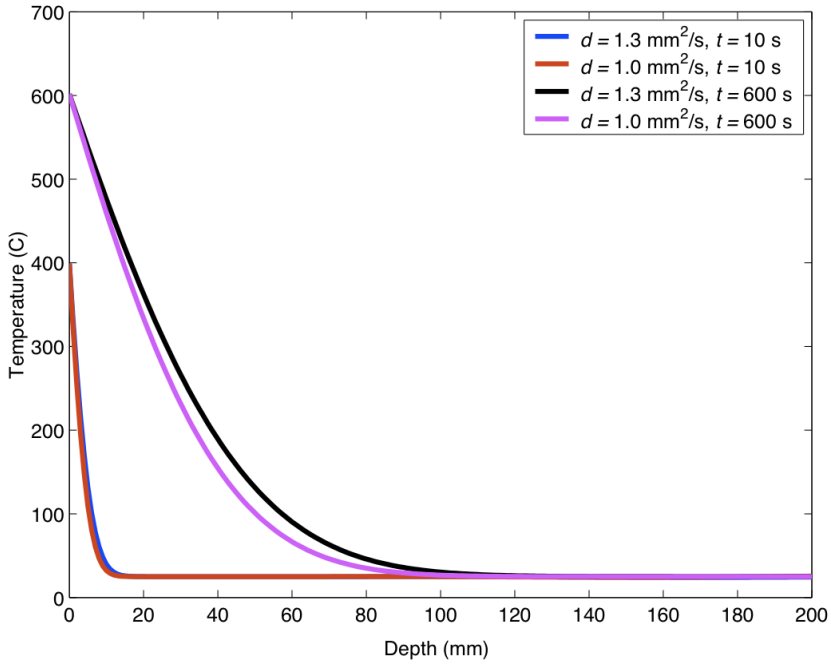

Figure 2.2: **Concrete Pavement Temperature Profile at $t = 10$ s and $t = 600$ s Due to Fast Transient Thermal Loadings**

2.1.2 Section Summary

In this section, rapidly varying 1-D temperature profiles in a homogeneous half-space subjected to transient thermal loadings are investigated. The well-known general solution for this problem is numerically evaluated using efficient Gaussian-type integration formulas developed by Steen et al.[11] Numerical calculations based on a uniform initial pavement temperature profile and a model surface temperature history are carried out, and match well with published results.

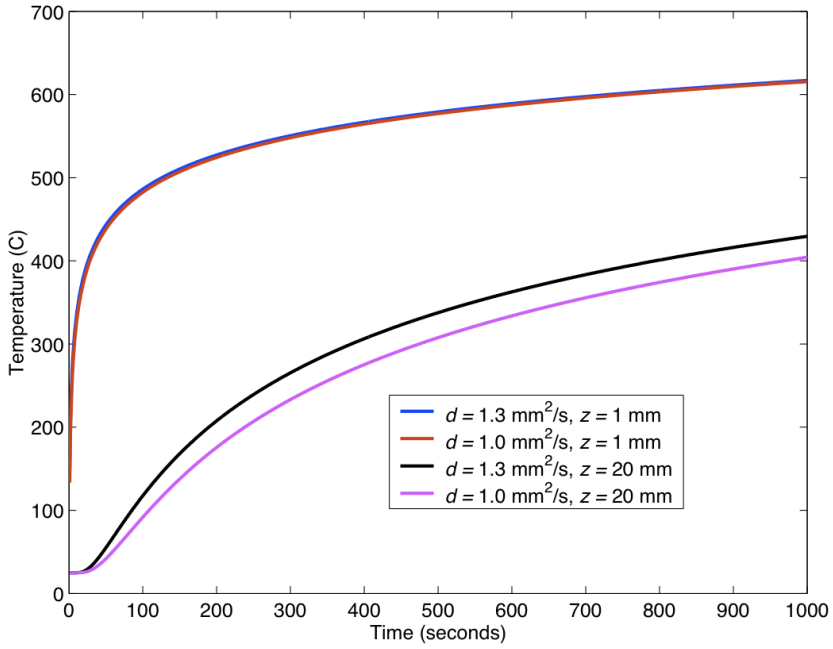

Figure 2.3: **Transient Temperature Values at $z = 1$ mm and $z = 20$ mm at Different Times Due to Fast Transient Thermal Loadings**

2.2 1-D Temperature Field in Two-layered Pavement Systems Subjected to High-Temperature Transient Loadings

The 1-D time-dependent temperature profile in a homogeneous half-space can be extended to a two-layered pavement system, as shown in Figure 2.4. This idealized two-layered system can be eventually used to analyze a heat-resistant concrete layer over a conventional concrete layer. Again, the temperature profile in a two-layered system can be modeled as an initial-boundary-value problem, where h_1 = thickness of Portland cement concrete (m); h_2 = thickness of the base layer (m); λ_j = thermal conductivity of the jth layer (kcal/m h °C); α_j = thermal diffusivity of the jth layer (m^2/h); and $T_j(z,t)$ = temperature function for layer j (°C). The material in each layer is assumed to be continuous, homogeneous, and isotropic. The temperature $T_2(z,t)$ is assumed to be constant for $z \geq H_2$ and $t > 0$.

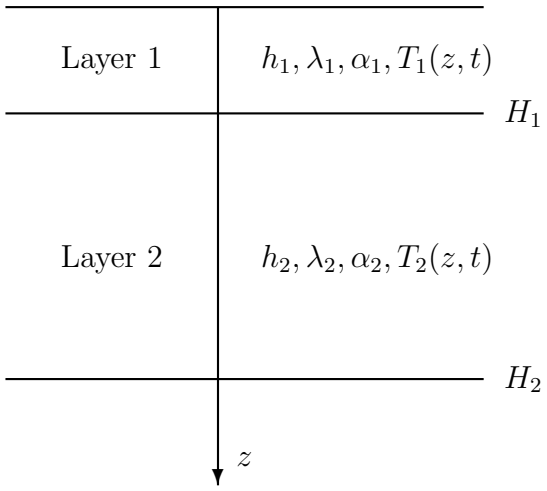

Figure 2.4: **Two-layered Pavement System**

2.2.1 Specified Pavement Surface Temperature

Similar to Section 2.1, suppose that the measured transient surface temperature data is available, then 1-D time-dependent temperature profile in a two-layered pavement system subjected to this high temperature transient loadings can be modeled as the following initial boundary value problem

$$\begin{aligned}
\frac{\partial T_j}{\partial t}(z,t) &= \alpha_j \frac{\partial^2 T_j}{\partial z^2}(z,t) \qquad 0 < t < \infty, \qquad H_{j-1} < z < H_j, \quad j = 1,2 \\
T_j(z,0) &= G_j(z), \qquad j = 1,2 \qquad \text{(initial condition)} \\
T_1(0,t) &= F(t) \qquad \text{(first boundary condition)} \\
T_2(H_2,t) &= \text{constant} \qquad \text{(second boundary condition)} \\
T_1(H_1,t) &= T_2(H_1,t) \qquad \text{(first interface condition)} \\
\lambda_1 \frac{\partial T_1}{\partial z}(H_1,t) &= \lambda_2 \frac{\partial T_2}{\partial z}(H_1,t) \qquad \text{(second interface condition)}
\end{aligned} \tag{2.11}$$

where $H_0 = 0,\ H_1 = h_1$ and $H_2 = h_1 + h_2$.

The main mathematical tool used for solving the system (2.11) is a LT. To facilitate the derivation of the solution, we introduce the variable $U_j(z,t),\ j=1,2$ below

$$U_j(z,t) = T_j(z,t) - T_j(z,0) \tag{2.12}$$

For simplicity, we assume that the initial temperature, $T_j(z,0),\ j=1,2$ is a constant. From Equation (2.12), the system (Equation 2.11) can be written as the following initial-boundary-value problem:

$$\begin{aligned}
\frac{\partial U_i}{\partial t}(z,t) &= \alpha_i \frac{\partial^2 U_i}{\partial z^2}(z,t) \qquad 0<t<\infty, \quad H_{i-1}<z<H_i, \quad i=1,2 && (2.13)\\
U_i(z,0) &= 0 && (2.14)\\
U_1(0,t) &= F(t) - T_1(0,0) && (2.15)\\
U_2(H_2,t) &= 0 && (2.16)\\
U_1(H_1,t) &= U_2(H_1,t) && (2.17)\\
\lambda_1 \frac{\partial U_1}{\partial z}(H_1,t) &= \lambda_2 \frac{\partial U_2}{\partial z}(H_1,t) && (2.18)
\end{aligned}$$

and we assume that $T_2(H_2,t) = T_2(H_2,0)$ for all $t>0$.

Let $\mathcal{L}$ denote the LT operator and $\hat{U}_i(z,s)$ be the LT of $U_i(z,t)$ with respect to time t. Furthermore, the following operational property[12] of LT is needed:

$$\mathcal{L}\left[f'(t)\right] = s\hat{f}(s) - f(0) \tag{2.19}$$

where $\hat{f}(s)$ is assumed to exist.

Applying LT with respect to t to Equation (2.13) in conjunction with Equations (2.14) and (2.19) yields

$$\frac{\partial^2 \hat{U}_j(z,s)}{\partial z^2} - \frac{s}{\alpha_j}\hat{U}_j(z,s) = 0, \qquad H_{j-1}<z<H_j,\ j=1,2 \tag{2.20}$$

If we let $r_j(s) = \sqrt{\frac{s}{\alpha_j}}$, then the solution of Equation (2.20) is

$$\hat{U}_j(z,s) = A_j(s)e^{-r_j z} + B_j(s)e^{r_j z},\ j = 1,2 \tag{2.21}$$

where $A_j(s),\ B_j(s),\ j = 1,2$ are to be determined using LT of boundary and interface conditions. Applying LT with respect to t to the boundary and interface conditions in Equations (2.15)–(2.18) yields Equations (2.22)–(2.25), respectively:

$$\begin{aligned}
\hat{U}_1(0,s) &= \hat{F}(s) - \frac{c}{s} && (2.22)\\
\hat{U}_2(H_2,s) &= 0 && (2.23)\\
\hat{U}_1(H_1,s) &= \hat{U}_2(H_1,s) && (2.24)\\
\lambda_1\frac{\partial\hat{U}_1}{\partial z}(H_1,s) &= \lambda_2\frac{\partial\hat{U}_2}{\partial z}(H_1,s) && (2.25)
\end{aligned}$$

where the constant c stands for $T_1(0,0)$.

From Equation (2.21), we know

$$\frac{\partial\hat{U}_j}{\partial z}(z,s) = -r_j A_j(s)e^{-r_j z} + r_j B_j(s)e^{r_j z},\ j = 1,2 \tag{2.26}$$

Substituting Equations (2.21) and (2.26) into Equations (2.22)–(2.25) yields the following linear system in which $A_j(s),\ B_j(s),\ j = 1,2$ are unknown variables

$$\begin{bmatrix} a_{11} & a_{12} & 0 & 0 \\ a_{21} & a_{22} & a_{23} & a_{24} \\ a_{31} & a_{32} & a_{33} & a_{34} \\ 0 & 0 & a_{43} & a_{44} \end{bmatrix} \begin{bmatrix} A_1(s) \\ B_1(s) \\ A_2(s) \\ B_2(s) \end{bmatrix} = \begin{bmatrix} C_1 \\ 0 \\ 0 \\ 0 \end{bmatrix} \tag{2.27}$$

where

$$
\begin{array}{llll}
a_{11} = 1 & a_{12} = 1 & & \\
a_{21} = e^{-r_1 H_1} & a_{22} = e^{r_1 H_1} & a_{23} = -e^{-r_2 H_1} & a_{24} = -e^{r_2 H_1} \\
a_{31} = -\lambda_1 r_1 e^{-r_1 H_1} & a_{32} = \lambda_1 r_1 e^{r_1 H_1} & a_{33} = \lambda_2 r_2 e^{-r_2 H_1} & a_{34} = -\lambda_2 r_2 e^{r_2 H_1} \\
a_{43} = e^{-r_2 H_2} & a_{44} = e^{r_2 H_2} & & \\
C_1 = \hat{F}(s) - \frac{c}{s} & & &
\end{array}
\tag{2.28}
$$

The linear system (Equation 2.27) can be easily solved by using Cramer's rule to give

$$
\begin{aligned}
A_1(s) &= \frac{C_1}{\Delta} I_1 \\
B_1(s) &= -\frac{C_1}{\Delta} I_2 \\
A_2(s) &= 2\frac{C_1}{\Delta} \lambda_1 r_1 e^{r_2 H_2} \\
B_2(s) &= -2\frac{C_1}{\Delta} \lambda_1 r_1 e^{-r_2 H_2}
\end{aligned}
\tag{2.29}
$$

where

$$
\begin{aligned}
I_1 &= e^{r_1 h_1} \left[\lambda_1 r_1 \sinh(r_2 h_2) + \lambda_2 r_2 \cosh(r_2 h_2)\right] \\
I_2 &= e^{-r_1 h_1} \left[-\lambda_1 r_1 \sinh(r_2 h_2) + \lambda_2 r_2 \cosh(r_2 h_2)\right] \\
\Delta &= 2\left[\lambda_1 r_1 \sinh(r_2 h_2)\cosh(r_1 h_1) + \lambda_2 r_2 \cosh(r_2 h_2)\sinh(r_1 h_1)\right] \\
h_2 &= H_2 - H_1
\end{aligned}
$$

From Equation (2.4) in Section 2.1, it is clear that $T_s(t)$ can be well approximated for large t by

$$
F(t) = 285 + 49.5 \ln(t), \quad t > 1 \tag{2.30}
$$

Since the LT of Equation (2.30) is much simpler than that of (2.4), Equation (2.30) will be

used in the following sample calculation. The LT of $\ln(t)$ takes the form[13]

$$L[\ln(t)] = -\frac{\gamma + \ln(s)}{s} \tag{2.31}$$

where $\gamma \approx 0.5772156$ is Euler's constant.

In view of Equation (2.31), the LT of Equation (2.30) is

$$\hat{F}(s) = \frac{285 - 49.5(\gamma + \ln(s))}{s} \tag{2.32}$$

Based on $T_j(z, 0) = 25,\ j = 1, 2$ (see Equation (2.5)) and Equation (2.32), C_1 can be obtained as

$$C_1 = \frac{1}{s}\left[260 - 49.5(\gamma + \ln(s))\right] \tag{2.33}$$

Substituting $A_j(s), B_j(s),\ j = 1, 2$ in Equation (2.29) into Equation (2.21) and using the inverse LT yields

$$U_1(z,t) = \frac{1}{2\pi i}\int_{\nu-i\infty}^{\nu+i\infty} \hat{U}_1(z,s)e^{st}ds, \quad 0 < z < H_1 \tag{2.34}$$

$$U_2(z,t) = \frac{1}{2\pi i}\int_{\nu-i\infty}^{\nu+i\infty} \hat{U}_2(z,s)e^{st}ds, \quad H_1 < z < H_2 \tag{2.35}$$

where ν is some real number such that $\hat{U}_j(z, s),\ j = 1, 2$ converges absolutely along the line $\mathrm{Re}(s) = \nu$, where $\mathrm{Re}(s)$ denotes[14] the real part of a complex number s.

Due to the complexities of $\hat{U}_j(z, s),\ j = 1, 2$, the closed-form solutions of Equations (2.34) and (2.35) are difficult to derive, so we seek numerical inversion of the LT. In this study, the Gaussian quadrature formula[15] for evaluating the following integral of functions of complex variables is employed

$$\frac{1}{2\pi i}\int_{\nu-i\infty}^{\nu+i\infty} \frac{e^p}{p} F(p)\, dp \approx \sum_{j=1}^{N} w_j F(p_j) \tag{2.36}$$

where $N \geq 2$ is an integer; $w_j, p_j, j = 1, 2, \ldots, N$ are weights and abscissae, respectively.

For the sake of completeness, $p_j, w_j,\ j = 1, 3, \ldots, 9$ are listed in Table 2.3, and $p_j,\ w_j$ are equal to the conjugate of p_{j-1}, w_{j-1} for $j = 2, 4, \ldots, 10$, respectively.[15]

Table 2.3: **Abscissae and Weights Used in The 10-point Gaussian Quadrature Formula**

i	p_i	w_i
1	12.83767707781087 + 1.666062584162301i	-868.4606112670226 + 15457.42053305275i
3	12.22613148416215 + 5.012719263676864i	1551.634444257753 - 8439.832902983925i
5	10.93430343060001 + 8.409672996003092i	-858.6520055271992 + 2322.065401339348i
7	8.776434640082609 + 11.92185389830121i	186.3271916070924 - 253.3223820180114i
9	5.225453367344361 + 15.72952904563926i	-10.34901907062327 + 4.110935881231860i

For fixed z and t, let $st = p$. Then complex integrals in Equations (2.34) and (2.35) can be written in the form of the integrals in Equation (2.36) as follows:

$$U_1(z,t) = \frac{1}{2\pi i}\int_{\gamma-i\infty}^{\gamma+i\infty} \frac{e^p}{p} F_1(p)\, dp, \quad 0 < z < H_1 \tag{2.37}$$

$$U_2(z,t) = \frac{1}{2\pi i}\int_{\gamma-i\infty}^{\gamma+i\infty} \frac{e^p}{p} F_2(p)\, dp, \quad H_1 < z < H_2 \tag{2.38}$$

where $F_j(p) = \hat{U}_j(z, \frac{p}{t})\frac{p}{t},\ j = 1, 2$. Then Equations (2.37) and (2.38) can be approximated using Eq. (2.36). To verify the validity of applying Equation (2.36) to evaluate Equations (2.37) and (2.38), a sample calculation was performed using parameters given in Table 2.4.

Table 2.4: **Geometry and Material Parameters Used in the Sample Calculation**

Parameters	Value
Layer thickness (m)	
h_1	0.4
h_2	2.0
Thermal conductivity, λ (kcal/m h °C)	
PCC slab	1.85
Base layer	1.20
Thermal diffusivity, α (m^2/h)	
PCC slab	0.00468
Base layer	0.00360

In the sample calculation, it is assumed that $T_j(z,0) = 25\ ^\circ\text{C}$, $j = 1, 2$, so in view of Equation (2.12), the final solution $T_j(z,t),\ j = 1, 2$ is

$$T_j(z,t) = U_j(z,t) + 25 \tag{2.39}$$

Figure 2.5 plots temperature profiles in the concrete slab at time t = 10, 60, 180, 360 and 600 s using temperature solutions for a two-layered system; Figure 2.6 illustrates transient temperature histories from t = 1 to 1000 s at z = 1, 10, 20, 50, 100 and 200 mm measured from pavement surface.

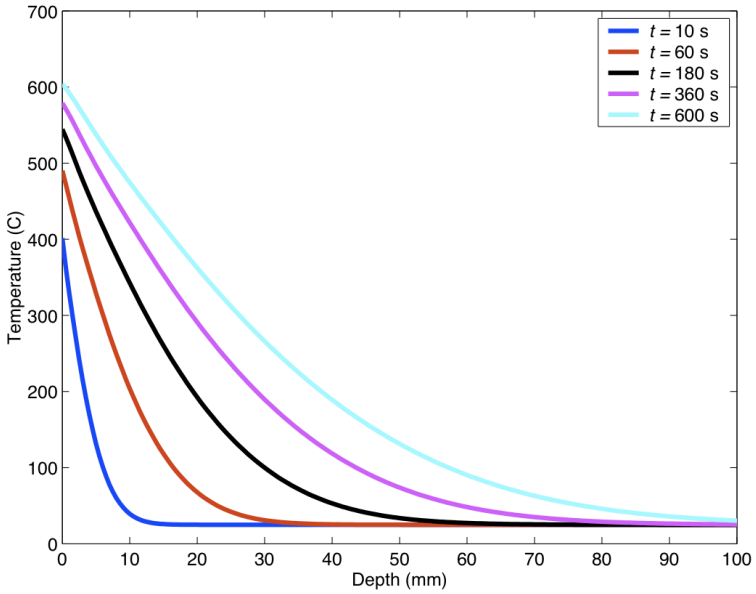

Figure 2.5: **Transient Concrete Slab Temperature Profile for a Two-layered System Subjected to Transient Thermal Loading**

2.2.2 Specified Heat Flux from Aircraft Engine, $Q(t)$

In this case, we assume that if the heat flux emanating from aircraft engine, $Q(t)$, is known, then the underlying mathematical model to estimate the 1-D temperature field in a two-

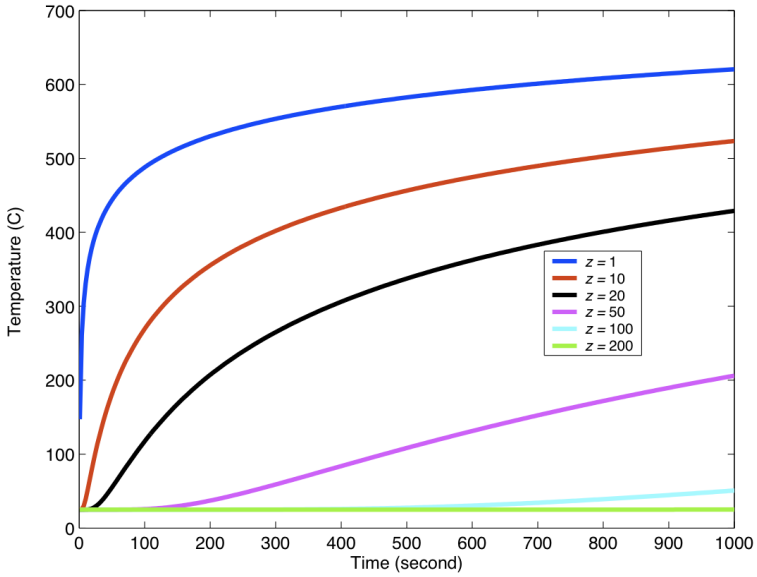

Figure 2.6: **Transient Temperature Values Evaluated at Different Depths in the Concrete Slab for a Two-layered System Subjected to Thermal Loading**

layered pavement system, as shown in Figure 2.4, is given by the following equations:

$$
\begin{aligned}
\frac{\partial T_j}{\partial t}(z,t) &= \alpha_j \frac{\partial^2 T_j}{\partial z^2}(z,t) \qquad 0 < t < \infty, \qquad H_{j-1} < z < H_j, \quad j = 1,2 \\
T_j(z,0) &= G_j(z), \qquad j = 1,2 \qquad \text{(initial condition)} \\
-\lambda_1 \frac{\partial T_1}{\partial z}(0,t) &= B\left[\frac{Q(t)}{B} + T_{\text{air}}(t) - T_1(0,t)\right] \qquad \text{(first boundary condition)} \\
T_2(H_2,t) &= \text{constant} \qquad \text{(second boundary condition)} \\
T_1(H_1,t) &= T_2(H_1,t) \qquad \text{(first interface condition)} \\
\lambda_1 \frac{\partial T_1}{\partial z}(H_1,t) &= \lambda_2 \frac{\partial T_2}{\partial z}(H_1,t) \qquad \text{(second interface condition)}
\end{aligned}
\tag{2.40}
$$

where $B =$ pavement surface convection coefficient (kcal/m^{2}hr °C); $T_{\text{air}}(t) =$ air temperature (°C); and the other variables are defined in Section 2.2.1. Note that the heat input from direct solar radiation is ignored in this problem due to the rapid transient heating of the surface by the aircraft engines. The only difference between Systems (2.11) and (2.40) is the first boundary condition.

Similar to Section 2.2.1, let $U_j(z,t) = T_j(z,t) - T_j(z,0),\ j = 1,2$ and suppose that $T_j(z,0)$ is a constant, then the first boundary condition in System (2.40) becomes

$$-\lambda_1 \frac{\partial U_1}{\partial z}(0,t) = B\left[\frac{Q(t)}{B} + T_{\text{air}}(t) - T_1(0,0) - U_1(0,t)\right] \tag{2.41}$$

Since $\frac{Q(t)}{B} \gg T_{\text{air}}(t) - T_1(0,0)$, we can drop $T_{\text{air}}(t) - T_1(0,0)$ for simplicity. Thus System (2.40) can be rewritten in terms of $U_j(z,t), j = 1,2$ as follows:

$$\begin{aligned}
\frac{\partial U_j}{\partial t}(z,t) &= \alpha_j \frac{\partial^2 U_j}{\partial z^2}(z,t) \qquad 0 < t < \infty, \quad H_{j-1} < z < H_j, \quad j = 1,2 && (2.42)\\
U_j(z,0) &= 0 && (2.43)\\
-\lambda_1 \frac{\partial U_1}{\partial z}(0,t) &= Q(t) - BU_1(0,t) && (2.44)\\
U_2(H_2,t) &= 0 && (2.45)\\
U_1(H_1,t) &= U_2(H_1,t) && (2.46)\\
\lambda_1 \frac{\partial U_1}{\partial z}(H_1,t) &= \lambda_2 \frac{\partial U_2}{\partial z}(H_1,t) && (2.47)
\end{aligned}$$

where it is assumed that $T_2(H_2,t) = T_2(H_2,0)$ for all t.

Similar to Section 2.2.1, the main mathematical tools employed to resolve the system in equation (2.40) are again a LT and the numerical inversion of a LT. Referring to Section 2.2.1, $\hat{U_j}(z,s),\ j = 1,2$ are given by Equation (2.21) with $A_j(s), B_j(s),\ j = 1,2$ determined using a LT of boundary and interlayer contact conditions. Applying a LT to Equation (2.44) with respect to t gives

$$-\lambda_1 \frac{\partial \hat{U_1}}{\partial z}(0,s) = \hat{Q}(s) - B\hat{U_1}(0,s) \tag{2.48}$$

In the following sample calculation, $Q(t)$, the step function representing the heat flux emanated from the aircraft engines, is assumed to be given by

$$Q(t) = \begin{cases} Q_0 & \text{if } t_1 \le t \le t_2 \\ 0 & \text{if } 0 \le t < t_1 \text{ or } t > t_2 \end{cases} \tag{2.49}$$

where Q_0 is a constant heat flux; t_1, t_2 are two time values. Thus, the LT of Equation (2.49) is

$$\hat{Q}(s) = \frac{Q_0}{s}\left(e^{-st_1} - e^{-st_2}\right) \tag{2.50}$$

As in Section 2.2.1, $A_j(s)$, $B_j(s)$, $j = 1, 2$ can be determined using the linear system (2.27) with all the symbols defined in Equation (2.28) except the following:

$$\begin{aligned} a_{11} &= B + \lambda_1 r_1 \\ a_{12} &= B - \lambda_1 r_1 \\ C_1 &= \frac{Q_0}{s}\left(e^{-st_1} - e^{-st_2}\right) \end{aligned} \tag{2.51}$$

and $A_j(s)$, $B_j(s)$, $j = 1, 2$ are given as follows:

$$\begin{aligned} A_1(s) &= \frac{C_1}{\widetilde{\Delta}}\widetilde{I}_1 \\ B_1(s) &= -\frac{C_1}{\widetilde{\Delta}}\widetilde{I}_2 \\ A_2(s) &= 2\frac{C_1}{\widetilde{\Delta}}\lambda_1 r_1 e^{h_1(r_2 - r_1)} \\ B_2(s) &= -2\frac{C_1}{\widetilde{\Delta}}\lambda_1 r_1 e^{-2r_2h_2 - h_1(r_1 + r_2)} \end{aligned} \tag{2.52}$$

where

$$\begin{aligned} \widetilde{I}_1 &= \lambda_1 r_1 + \lambda_2 r_2 + (\lambda_2 r_2 - \lambda_1 r_1)\, e^{-2r_2h_2} \\ \widetilde{I}_2 &= (\lambda_2 r_2 - \lambda_1 r_1)\, e^{-2r_1h_1} + (\lambda_1 r_1 + \lambda_2 r_2)\, e^{-2(r_1h_1 + r_2h_2)} \\ \widetilde{\Delta} &= (B + \lambda_1 r_1)\left[\lambda_1 r_1 + \lambda_2 r_2 + (\lambda_2 r_2 - \lambda_1 r_1)e^{-2r_2h_2}\right] \\ &\quad + (B - \lambda_1 r_1)e^{-2r_1h_1}\left[\lambda_1 r_1 - \lambda_2 r_2 - (\lambda_1 r_1 + \lambda_2 r_2)e^{-2r_2h_2}\right] \end{aligned} \tag{2.53}$$

Table 2.5: **Additional Parameters Assumed in The Sample Calculation**

Parameters	Value
B (kcal/m^2 h °C)	16.29
Q_0 (kcal/m^2 h)	90,000
$T_j(z,0),\ j=1,2$ (°C)	25
Time variables used in $Q(t)$ (s)	
t_1	10
t_2	130

Furthermore, inserting Equation (2.52) into Equation (2.21) yields $\hat{U}_j(z,s),\ j=1,2$ below

$$\begin{aligned}\hat{U}_1(z,s) &= \frac{C_1}{\widetilde{\Delta}}\left\{(\lambda_1 r_1+\lambda_2 r_2)e^{-r_1 z}\left[1-e^{-2(r_1h_1+r_2h_2-r_1z)}\right]\right.\\ &\quad \left.+(\lambda_2 r_2-\lambda_1 r_1)\left[e^{-(2r_2h_2+r_1z)}-e^{-2r_1h_1+r_1z}\right]\right\} \qquad (2.54)\\ \hat{U}_2(z,s) &= \frac{C_1}{\widetilde{\Delta}}2\lambda_1 r_1 e^{-r_2(z-h_1)-r_1h_1}\left[1-e^{-2r_2(H_2-z)}\right] \qquad (2.55)\end{aligned}$$

where C_1 is given in Equation (2.51).

As in Section 2.2.1, $U_j(z,t),\ j=1,2$ can be determined by an inverse LT as in Equations (2.34) and (2.35). The numerical inversion can be estimated using the 10-point Gaussian quadrature formula shown in Equation (2.36). In the sample calculation, the parameters from Table 2.4 are selected in addition to those given in Table 2.5.

Figure 2.7 plots temperature profiles in the concrete slab at time t = 15, 30, 60, 90, 120, 150, and 210 s using temperature solutions for a two-layered pavement system in this section. Figure 2.8 illustrates transient temperature histories from t = 1 to 1000 s at z = 0, 1, 3, 5, 8, 10, 20, 30, and 40 mm measured from pavement surface.

2.2.3 Sensitivity Study

In this subsection, we conduct a brief sensitivity study of the effects of thermal properties and the thickness of the first layer on the temperature profile in a two-layered system. This will give some clues to the selection of appropriate materials having heat-resistant properties

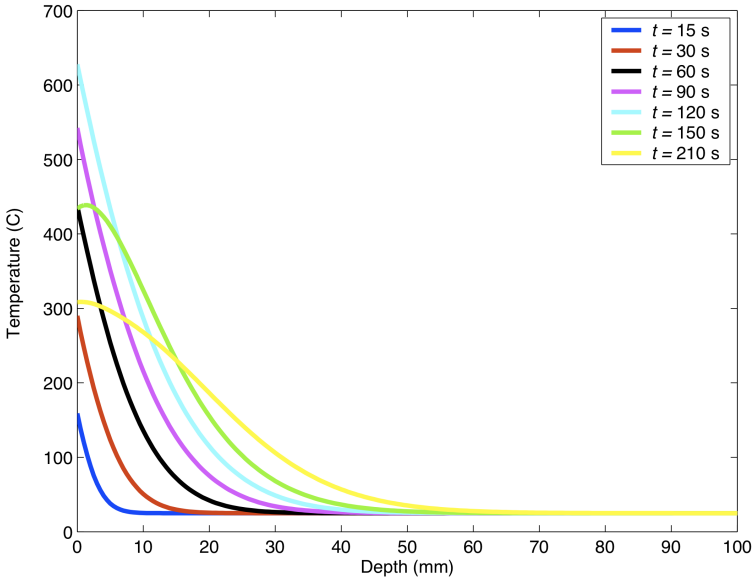

Figure 2.7: **Transient Concrete Slab Temperature Profile in The First Layer for a Two-layered Pavement System Subjected to Specified Heat Flux from Aircraft**

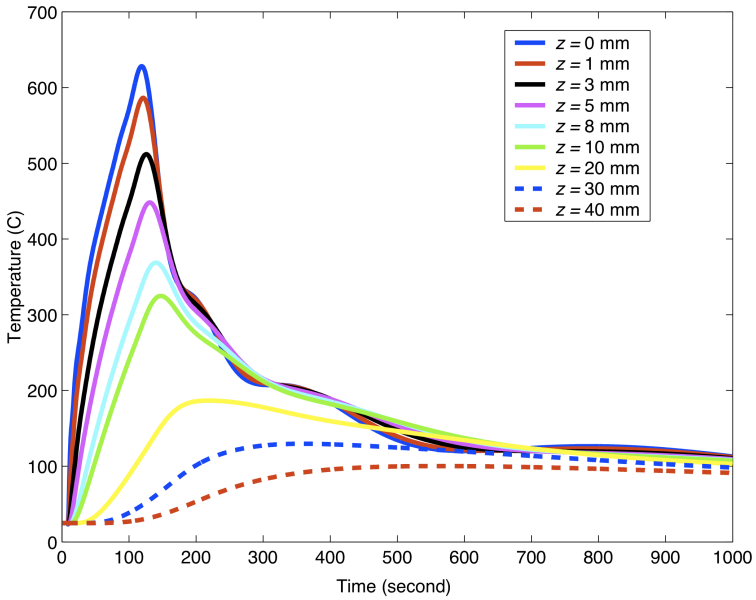

Figure 2.8: **Transient Temperature Values Evaluated at Different Depths in The First Layer for a Two-layered Pavement System Subjected to Specified Heat Flux from Aircraft**

Table 2.6: **Geometry and Material Parameters Used in The Sensitivity Study**

Parameters	Value
Layer thickness (mm)	
h_1	60,100
h_2	400
Thermal conductivity, λ (kcal/mm s °C)	
Geopolymer paste	$2.0\text{x}10^{-7}$
PCC slab	$5.1\text{x}10^{-7}$
Thermal diffusivity, α (mm^2/s)	
Geopolymer	0.2
PCC slab	1.3

for the surface layer of airfield concrete pavements. Geopolymer materials have desirable properties for serving as an alternative binder to traditional Portland cement in producing paving concrete. These properties include lower thermal conductivity and diffusivity values, high compressive strength at early age, non-flammability, and high thermal stability. Thus it is possible to construct paving concrete made from a geopolymer binder on top of the ordinary concrete slab to limit temperature penetration into the ordinary concrete layer.[16] The following sensitivity study gives an example of such a two-layered system.

The parameters used in the sensitivity study are given in Tables 2.5 and 2.6. Figures 2.9 and 2.10 plot temperature profiles at different times, and Figures 2.11 and 2.12 plot transient temperature values evaluated at different depths, for a two-layered system with $h_1 = 60$ mm and $h_1 = 100$ mm. Actual calculations show that there are no differences in the first nine significant digits between calculated temperature values in generating Figures 2.9–2.12, i.e., fixing all the other parameters and replacing $h_1 = 60$ mm by $h_1 = 100$ mm does not change temperature profiles in the two-layered system under the rapidly imposed thermal loading case. However, Figures 2.8 and 2.11 demonstrate that the peak temperature values in the two-layered system containing geopolymer materials are lower than those in the ordinary concrete two-layered system at all depths except the surface, as expected. In particular, at $z = 40$ mm, the peak temperature drops from around 100 °C in Figure 2.8 to about 37 °C

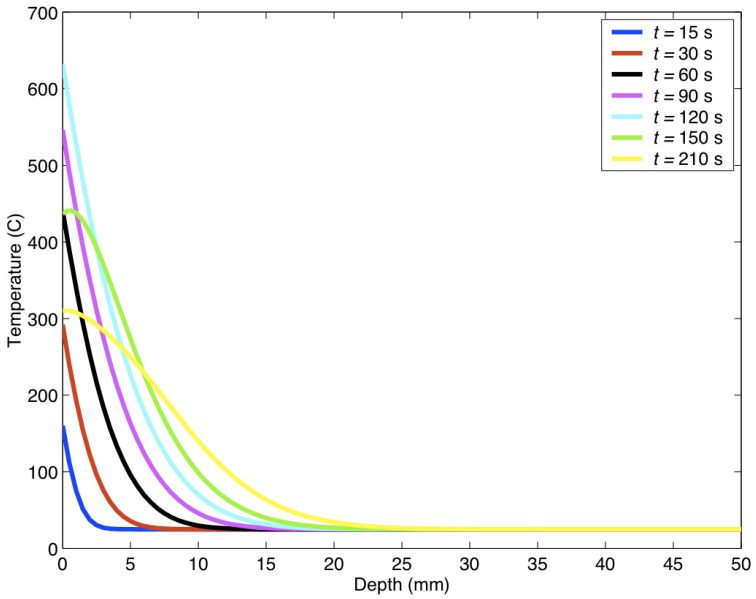

Figure 2.9: **Transient Temperature Profile for a Geopolymer-concrete System ($h_1 = 60$ mm) Subjected to Specified Heat Flux from Aircraft Operation**

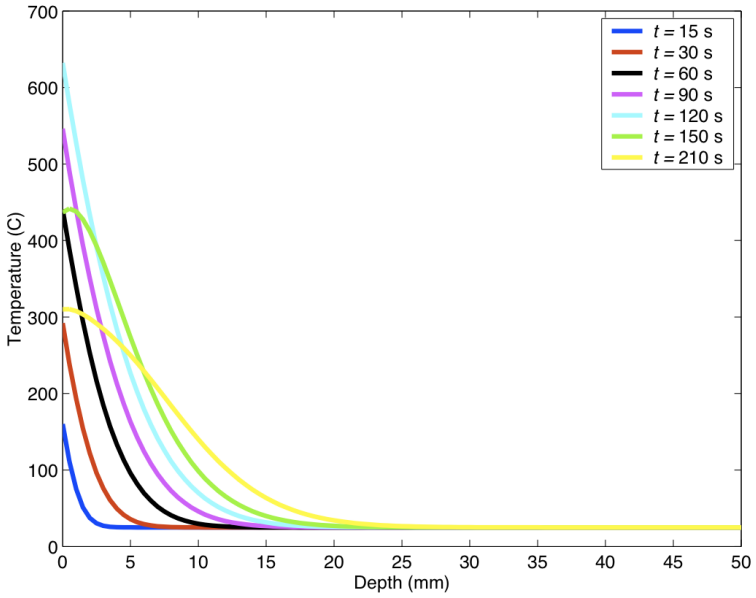

Figure 2.10: **Transient Temperature Profile for a Geopolymer-concrete System ($h_1 = 100$ mm) Subjected to Specified Heat Flux from Aircraft Operation**

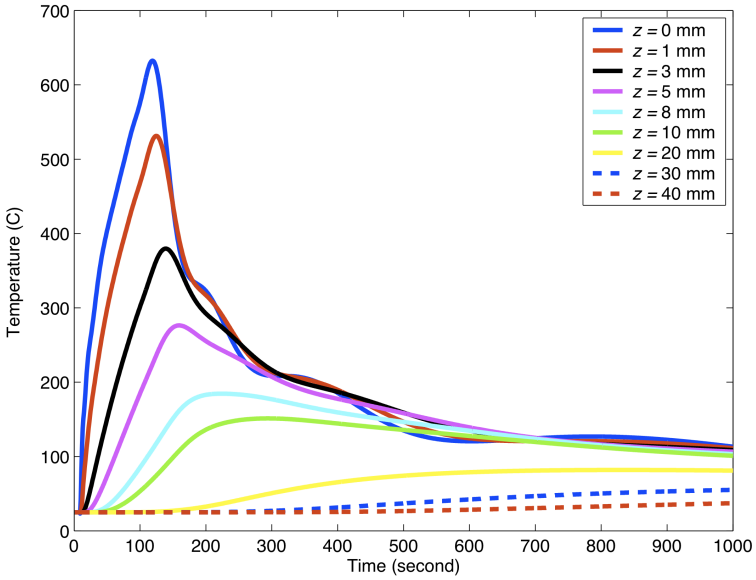

Figure 2.11: **Transient Temperature Values Evaluated at Different Depths in a Geopolymer-concrete System ($h_1 = 60$ mm) Subjected to Specified Heat Flux from Aircraft Operation**

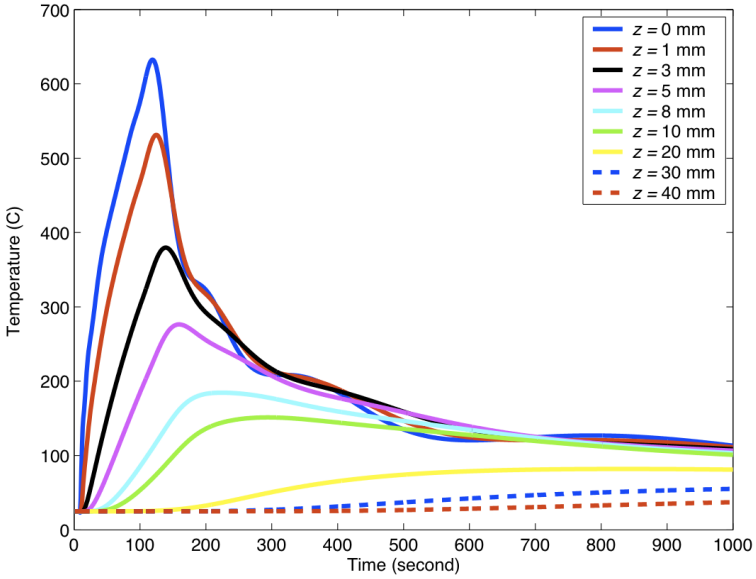

Figure 2.12: **Transient Temperature Values Evaluated at Different Depths in a Geopolymer-concrete System ($h_1 = 100$ mm) Subjected to Specified Heat Flux from Aircraft Operation**

in Figure 2.11.

2.2.4 Section Summary

In this section, 1-D rapidly varying temperature profiles in two-layered pavement systems subjected to transient thermal loadings were studied. The underlying solution techniques were LT and numerical inverse LT. Analytical solutions were derived for both the specified surface temperature history and the heat flux from aircraft engine conditions. Numerical calculations were carried out to illustrate the derived solutions. Also, a brief sensitivity study of the effects of material thermal properties and the thickness of the first layer on the temperature profile in a two-layered system was conducted.

Chapter 3

2-D AXISYMMETRIC FIELD IN HOMOGENEOUS HALF-SPACE

In this chapter, analytical solutions of a 2-D axisymmetric transient temperature field are derived under the assumption that the thermal loadings and surface boundary conditions are axisymmetric. To take advantage of axisymmetry, a cylindrical coordinate system is used, as shown in Figure 3.1, and α = thermal diffusivity (m^2/h) and $T(r, z, t)$ = the temperature function. Here, we assume that the surface temperatures are available during the period of interest. The mathematical formulation of this problem is given as

$$\frac{\partial T}{\partial t} = \alpha\left(\frac{\partial^2 T}{\partial r^2} + \frac{1}{r}\frac{\partial T}{\partial r} + \frac{\partial^2 T}{\partial z^2}\right), \qquad 0 < t < \infty, \qquad 0 < z < \infty \tag{3.1}$$

$$T(r, 0, t) = F(r, t), \qquad \text{(boundary condition)} \tag{3.2}$$

$$T(r, z, 0) = G(r, z), \qquad \text{(initial condition)} \tag{3.3}$$

where F and G are assumed to be continuous.

Let the time period of interest be $[0, t_\mathrm{e}]$, and m a positive integer. Suppose that $[0, t_\mathrm{e}]$ is divided into $2m$ sub-intervals of equal length, and that the surface temperature at $r = 0$ is measured at two end points of each sub-interval except at time t_e. Then the interpolatory trigonometric polynomials, based on the discrete least squares approximation, can be obtained to approximate $F(0, t)$ as follows[17]

$$F(0, t) = \frac{a_0}{2} + \frac{a_m}{2}\cos(m\bar{t}) + \sum_{k=1}^{m-1}\left[a_k \cos(k\bar{t}) + b_k \sin(k\bar{t})\right], \qquad 0 \le t \le t_\mathrm{e} - \frac{t_\mathrm{e}}{2m} \tag{3.4}$$

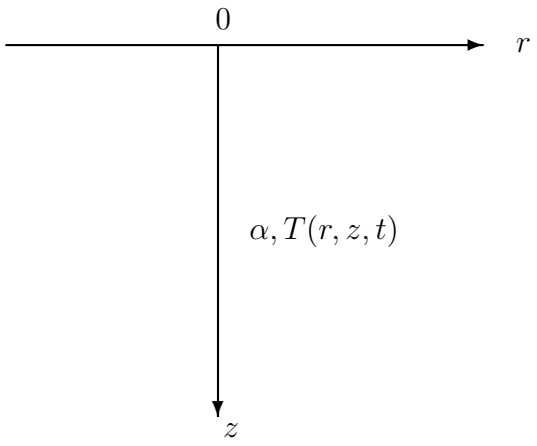

Figure 3.1: **Cylindrical Coordinate System**

with

$$\bar{t} = \pi\left(\frac{2t}{t_{\mathrm{e}}} - 1\right) \tag{3.5}$$

$$a_k = \frac{1}{m}\sum_{l=0}^{2m-1} T_l \cos\left[\frac{k\pi}{m}(l-m)\right] \quad \text{for each} \quad k = 0, 1, \ldots, m \tag{3.6}$$

$$b_k = \frac{1}{m}\sum_{l=0}^{2m-1} T_l \sin\left[\frac{k\pi}{m}(l-m)\right] \quad \text{for each} \quad k = 1, 2, \ldots, m-1 \tag{3.7}$$

where T_l = measured surface temperature at $r = 0$ at l^{th} partitioning point of $[0, t_{\mathrm{e}}]$, i.e., at time $t_l = \frac{l}{2m} t_{\mathrm{e}}$ for each $l = 0, 1, 2, \ldots, 2m-1$. In the following, $F(r, t)$ is assumed to have the form

$$F(r, t) = e^{-\mu r} F(0, t) \tag{3.8}$$

where μ is some parameter.

For simplicity, we assume that $T(r, z, 0)$ is independent of z. Also, the compatibilities of initial and boundary conditions at $z = 0, t = 0$ impose that $F(r, 0) = G(r, 0)$, which yields

$T(r,z,0) = F(r,0)$.

In view of the above discussion, the following focuses on the derivation of the analytical solution for $T(r,z,t)$ satisfying the partial differential equation (PDE) given in Equation (3.1) with the boundary and initial conditions given by

$$\begin{aligned} T(r,0,t) &= e^{-\mu r}\left\{\frac{a_0}{2}+\frac{a_m}{2}\sin\left[\frac{2m\pi}{t_e}t+\pi\left(\frac{1}{2}-m\right)\right]\right. \\ &\left.+\sum_{k=1}^{m-1}\left[a_k\sin\left(\frac{2k\pi}{t_e}t+\pi\left(\frac{1}{2}-k\right)\right)+b_k\sin\left(\frac{2k\pi}{t_e}t-k\pi\right)\right]\right\}, \end{aligned} \tag{3.9}$$

where $0 \le t \le t_e\left(1-\frac{1}{2m}\right)$; and

$$T(r,z,0) = e^{-\mu r}\left\{\frac{a_0}{2}+\frac{a_m}{2}\sin\left[\pi\left(\frac{1}{2}-m\right)\right]+\sum_{k=1}^{m-1}\left[a_k\sin\left(\pi\left(\frac{1}{2}-k\right)\right)+b_k\sin\left(-k\pi\right)\right]\right\}, \tag{3.10}$$

where Equation (3.10) is obtained by setting $t = 0$ in Equation (3.9). It is noted that Equation (3.1) is linear, so the principle of linear superposition implies that the final solution satisfying the Equations (3.1), (3.9) and (3.10) can be obtained by summing up each solution satifying Eq. (3.1) and the following boundary and initial conditions

$$T(r,0,t) = e^{-\mu r}A\sin(\omega t+\phi) \tag{3.11}$$

$$T(r,z,0) = e^{-\mu r}A\sin\phi \tag{3.12}$$

where we note that $e^{-\mu r}A\sin(\omega t+\phi)$ and $e^{-\mu r}A\sin\phi$ resemble the variable terms in the right hand side of Equations (3.9) and (3.10), respectively. Hence, the model initial-boundary-value problem consisting of Equations (3.1), (3.11) and (3.12) will be considered.

3.1 Separation of Variables

The method of SV has been employed to predict time-dependent temperature profiles in multilayered pavement systems using the measured air temperature, solar radiation intensity

and material parameters.[7] To facilitate the derivation of an analytical solution, the complex-valued function of real variables, $Y(r, z, t)$ is introduced, which is the solution of the following boundary value problem

$$\begin{aligned} \frac{\partial Y}{\partial t} &= \alpha\left(\frac{\partial^2 Y}{\partial r^2}+\frac{1}{r}\frac{\partial Y}{\partial r}+\frac{\partial^2 Y}{\partial z^2}\right), \qquad 0<t<\infty, \qquad 0<z<\infty \quad (3.13)\\ Y(r,0,t) &= Ae^{-\mu r+i(\omega t+\phi)} \quad (3.14)\\ Y(r,z,t) &\quad \text{is bounded} \quad (3.15)\end{aligned}$$

where i is the imaginary unit number with $i^2 = -1$.

It is clear that the imaginary part of $Y(r, z, t)$ satisfies the Equations (3.1) and (3.11), and in general does not satisfy the Equation (3.12). However, the influence of initial data $T(r, z, 0)$ on transient temperature distributions gradually decays as time increases,[9] and thus the solution based on the method of SV can still give a reasonable approximation to temperature at the point $Q(r, z, t)$ for small z and large t.

The following outlines the main steps involved in solving Equations (3.13) and (3.15) based on the method of separation of variables:

1. We assume that

$$Y(r,z,t) = u(r,z)e^{j(\omega t+\phi)} \quad (3.16)$$

then, it follows that

$$\frac{\partial Y}{\partial t} = j\omega Y \quad (3.17)$$

2. Inserting Equations (3.16) and (3.17) into Equation (3.13) yields

$$j\omega u = \alpha\left(\frac{\partial^2 u}{\partial r^2}+\frac{1}{r}\frac{\partial u}{\partial r}+\frac{\partial^2 u}{\partial z^2}\right) \quad (3.18)$$

3. We assume that u_r is bounded at $r = 0$, $u(r, z)$ is $O(r^{-k})$ [1] and $u_r(r, z)$ is $O(r^{-k+1})$ as $r \to \infty$ for each $z > 0$ with $k > \frac{3}{2}$. Then the HT of order zero of $u(r, z)$ with respect to r, $\bar{u}(\xi, z)$ defined below exists[19]

$$\bar{u}(\xi, z) = \int_0^\infty r u(r, z) J_0(\xi r) dr \tag{3.19}$$

where $J_0(\xi r)$ is a Bessel function of the first kind, of order zero.

Applying the HT on r to both sides of Equation (3.18), we obtain formally the following equation

$$\frac{\partial^2 \bar{u}}{\partial z^2}(\xi, z) - \left(\xi^2 + \frac{\omega}{\alpha} j\right) \bar{u}(\xi, z) = 0 \tag{3.20}$$

Note that the following fact was used in deriving Equation (3.20) when u and u_r satisfy the above-mentioned conditions[19]

$$\int_0^\infty r \left(\frac{d^2}{dr^2} + \frac{1}{r}\frac{d}{dr}\right) u(r, z) J_0(\xi r) dr = -\xi^2 \bar{u}(\xi, z) \tag{3.21}$$

4. Solving Equation (3.20), we find that

$$\bar{u}(\xi, z) = C e^{-\xi z(M + jN)} + D e^{\xi z(M + jN)} \tag{3.22}$$

where $M = \sqrt{\frac{V+1}{2}}$, $N = \sqrt{\frac{V-1}{2}}$, $V = \sqrt{1 + \left(\frac{\omega}{\alpha \xi^2}\right)^2}$; and C, D are constants of integration that are determined using the boundary condition.

5. The boundedness of $Y(r, z, t)$ implies $D = 0$ in Equation (3.22), and the inverse HT

[1] The order symbol O is defined as [18, pp. 570-571]

$$f(k) = O[G(K)], \quad k \to a \ \text{ (here } a \text{ may be } \pm\infty) \ \text{ if}$$

$$\text{absolute value of } \frac{F(k)}{G(k)} \text{ approaches to } A \text{ as } \ k \to a, \ \text{ where } A \text{ is a nonzero constant}$$

of $\bar{u}$ gives[19]

$$Y(r,z,t) = \int_0^\infty \xi C(\xi) e^{-\xi M z + j(\omega t - \xi N z + \phi)} J_0(\xi r) d\xi \tag{3.23}$$

6. Setting $z = 0$ in Equation (3.23) and considering Equation (3.14), we find that[19]

$$\begin{aligned} C(\xi) &= \int_0^\infty r A e^{-\mu r} J_0(\xi r) dr \\ &= A\mu(\xi^2 + \mu^2)^{-\frac{3}{2}} \end{aligned} \tag{3.24}$$

7. Substituting Equation (3.24) into Equation (3.23) yields the complete expression for $Y(r,z,t)$, whose imaginary part, $T(r,z,t)$, is the desired solution satisfying Equations (3.1) and (3.11)

$$T(r,z,t) = A\mu \int_0^\infty \frac{\xi}{(\xi^2 + \mu^2)^{3/2}} e^{-\xi M z} \sin(\omega t - \xi N z + \phi) J_0(\xi r) d\xi \tag{3.25}$$

It can be shown that for fixed t the improper integral in Equation (3.25) converges uniformly with respect to r and z, where $r \in [\,0, \infty\,)$ and $z \in [\,0, \infty\,)$ by using the Weierstrass criterion on uniform convergence of improper integrals involving parameters.[19]

In practice, the improper integral can be approximated using numerical integration schemes such as Gaussian quadrature formulas. However, the assumption in Equation (3.16) may not be valid even for moderate values of z under the condition of rapidly changing thermal loading, for example $z = 40$ mm as illustrated in Figure (3.6) below. Therefore, we propose another solution method based on integral transforms such as LT and HT.

3.2 Integral Transforms

In this section, we seek an analytical solution satisfying Equations (3.1), (3.11) and (3.12) based on LT and HT. The main steps involved in the derivation of solution are summarized as follows:

1. Refer to Section (2.2.1), Let $\hat{T}(r,z,s)$ denote the LT of $T(r,z,t)$ with respect to time t. Applying the LT with respect to t to both sides of Equation (3.1) yields

$$\frac{s}{\alpha}\hat{T}(r,z,s) - \frac{A}{\alpha}e^{-\mu r}\sin\phi = \frac{\partial^2\hat{T}}{\partial r^2} + \frac{1}{r}\frac{\partial\hat{T}}{\partial r} + \frac{\partial^2\hat{T}}{\partial z^2} \tag{3.26}$$

2. We assume that T_r is bounded at $r=0$, T is $O(r^{-k})$ and T_r is $O(r^{-k+1})$ as $r\to\infty$ for each $z>0$, $t>0$ with $k>\frac{3}{2}$. Applying the HT of order zero on r to both sides of Equation (3.26) produces the ordinary differential equation

$$\frac{d^2\bar{\hat{T}}}{dz^2} - \left(\xi^2 + \frac{s}{\alpha}\right)\bar{\hat{T}} = -\frac{A}{\alpha}\mu(\xi^2+\mu^2)^{-\frac{3}{2}}\sin\phi \tag{3.27}$$

   where $\bar{\hat{T}}(\xi,z,s)$ denote the HT of order zero of $\hat{T}(r,z,s)$.

3. The solution of Equation (3.27) is

$$\bar{\hat{T}}(\xi,z,s) = C(\xi,s)e^{-\beta z} + D(\xi,s)e^{\beta z} + \bar{\hat{T}}_p \tag{3.28}$$

   where $\beta = \sqrt{\xi^2+\frac{s}{\alpha}}$, $C(\xi,s)$ and $D(\xi,s)$ are constants of integration, and $\bar{\hat{T}}_p$ stands for a particular solution of Equation (3.27) and is given by

$$\bar{\hat{T}}_p = \frac{A\mu(\xi^2+\mu^2)^{-3/2}}{\alpha\xi^2+s}\sin\phi \tag{3.29}$$

4. Boundedness of $T(r,z,t)$ implies that for fixed complex number s with $\mathrm{Re}(s)>0$, $\hat{T}(r,z,s)$ is bounded for $r>0$, $z>0$, and it follows that $D(\xi,s)=0$. Thus

$$\bar{\hat{T}}(\xi,z,s) = C(\xi,s)e^{-\beta z} + \bar{\hat{T}}_p \tag{3.30}$$

   where $C(\xi,s)$ is to be determined using the BC.

5. Applying the LT on t to both sides of Equation (3.11) yields $\hat{T}(r,0,s)$

$$\hat{T}(r,0,s) = Ae^{-\mu r}\left(\frac{\omega}{\omega^2+s^2}\cos\phi + \frac{s}{\omega^2+s^2}\sin\phi\right) \tag{3.31}$$

Applying the HT of order zero on r to both sides of Equation (3.31) gives

$$\bar{\hat{T}}(\xi,0,s) = A\mu(\xi^2+\mu^2)^{-3/2}\left(\frac{\omega}{\omega^2+s^2}\cos\phi + \frac{s}{\omega^2+s^2}\sin\phi\right) \tag{3.32}$$

6. Setting $z = 0$ in Equation (3.30) and comparing with Equation (3.32) gives

$$C(\xi,s) = A\mu(\xi^2+\mu^2)^{-3/2}\left[\frac{\omega}{\omega^2+s^2}\cos\phi + \left(\frac{s}{\omega^2+s^2} - \frac{1}{\alpha\xi^2+s}\right)\sin\phi\right] \tag{3.33}$$

7. Substituting Equation (3.33) into Equation (3.30) and performing the inverse HT of order zero of $\bar{\hat{T}}(\xi,z,s)$ yields

$$\begin{aligned}\hat{T}(r,z,s) &= A\mu\int_0^\infty \xi(\xi^2+\mu^2)^{-3/2}\left\{\left[\frac{\omega}{\omega^2+s^2}\cos\phi + \left(\frac{s}{\omega^2+s^2} - \frac{1}{\alpha\xi^2+s}\right)\sin\phi\right]e^{-\beta z}\right. \\ &\quad \left. + \frac{1}{\alpha\xi^2+s}\sin\phi\right\} J_0(\xi r)d\xi \end{aligned} \tag{3.34}$$

8. Referring to Section 2.2.1, the final solution of $T(r,z,t)$ can be approximated using Equation (3.34) by numerical inverse LT methods such as Gaussian-Quadrature-type formulas.

3.3 Numerical Results

In this section, numerical results based on the above mentioned two solution methods are presented. In the following calculation, $\alpha = 0.0035$ m^2/h and $\mu = 0.01$ 1/m, and temperatures at $r = 0$ with $z = 0,\ 1,\ 5,\ 10,\ 20,\ 40,\ 60$ mm are calculated starting from $t = 0$ until $t = 1475$ s with an increment of 25 s.

The surface temperatures at $r = 0$ for every 25 s from $t = 0$ until $t = 1475$ s are generated using Figure 3.1 from Ju and Zhang.[2] Prescribed surface temperature values $T(0, 0, t)$ at $t = 0, 25, 50, \ldots, 1475$ s and those generated using the above mentioned interpolatory trigonometric polynomials are presented in Figure 3.2. When the approximation based on the method of SV is used, the surface temperatures $T(0, 0, t)$ are assumed to be $T(0, 0, 0)$ at each time $t = -300, -275, -250, \ldots, -50, -25$ s in order to get a more accurate solution of $T(r, z, 0)$ with $r \geq 0$ and $z > 0$.

For the numerical results based on the method of separation variables, the composite 16-point Gaussian quadrature formula is employed to evaluate Equation (3.25), replacing the upper limit ∞ by $\xi = 30$, which is determined using an error analysis. The length of each subinterval equals 0.2 in the composite Gaussian integration scheme, and the 10-point Guassian quadrature formula used for resolving inverse LT in Section 2.2.1 is employed again to obtain numerical values of $T(r, z, t)$.

Figure 3.3 shows the prescribed temperature $T(0, 0, t)$ at $t = 0, 25, 50, \ldots, 1475$ s and the predicted ones based on the methods of separation of variables and LT, respectively. Figure 3.3 indicates that the surface temperatures at $r = 0$ were almost exactly recovered by the results based on the method of SV, and well approximated for $t \leq 450$ s by results based on the LT. The artificial oscillation of temperature for the large t exhibited in the approximation based on the LT is probably caused by the error associated with the numerical inverse LT.

Figures 3.4–3.6 present the predicted transient temperature $T(0, z, t)$ at $z =$ 1,5,10,20,40,and 60 mm using the methods of separation of variables and LT, respectively, identified in Table 3.1. Figures 3.4–3.6 reveal that for $z = 1, 5, 10$ mm, the method of separation of variables gives a reasonable prediction of temperature except at small values of t, whereas the method of LT generates reasonable approximation except for artificial oscillations exhibited at $t > 700$ s, which are suspected to be caused by the numerical inverse LT. For $z = 20, 40, 60$ mm, LT gives better results than SV does. The reason behind this fact is that the latter does not use the initial temperature values and the assumption made in Equation (3.16)

Table 3.1: **Proposed Transient Temperature Prediction Using the Combined Solution Technique**

z (mm)	$T(0,z,t)$
0	based on SV
1	$T(0,1,0), T(0,1,25)$ based on LT, the others based on SV
5	$T(0,5,0), T(0,5,25), T(0,5,50)$ based on LT, the others based on SV
10	$T(0,10,0), T(0,10,25)$ based on LT, the others based on SV
20	based on LT
40	based on LT
60	based on LT

may not be valid in general.

To take advantage of the reasonable temperature prediction generated by each solution method, a combined solution technique is proposed in this study. For example, using the results presented in Figures 3.3–3.6, we proposed that the final approximation for the transient temperature at $z = 0, 1, 5, 10, 20, 40, 60$ mm, as shown in Figure 3.7, be generated using the approaches given in Table 3.1.

3.4 Section Summary

In this section, a 2-D axisymmetric temperature field with specified surface temperature history in a homogeneous half-space due to transient thermal loading is studied. Two solution methods are proposed, one based on the method of SV and HT, and the other based on LT and HT. Inverse HT and LT can be resolved numerically. A combined approach to a solution is proposed using results based on these two methods. Model calculations show that the combined solution approach gives a reasonable approximation to the rapidly varying temperature profile.

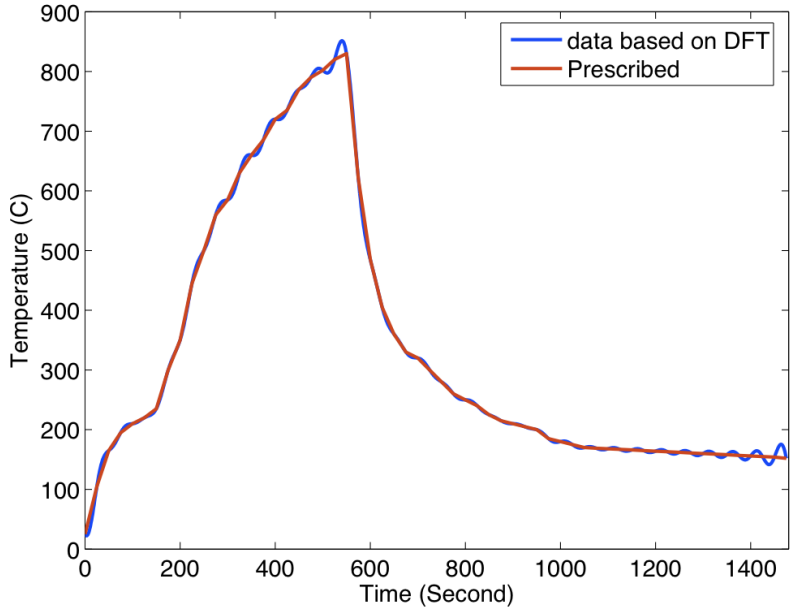

Figure 3.2: **Prescribed $T(0,0,t)$ at $t = 0, 25, 50, \ldots, 1475$ s and Its Predicted Values Based on The Interpolatory Trigonometric Polynomials**

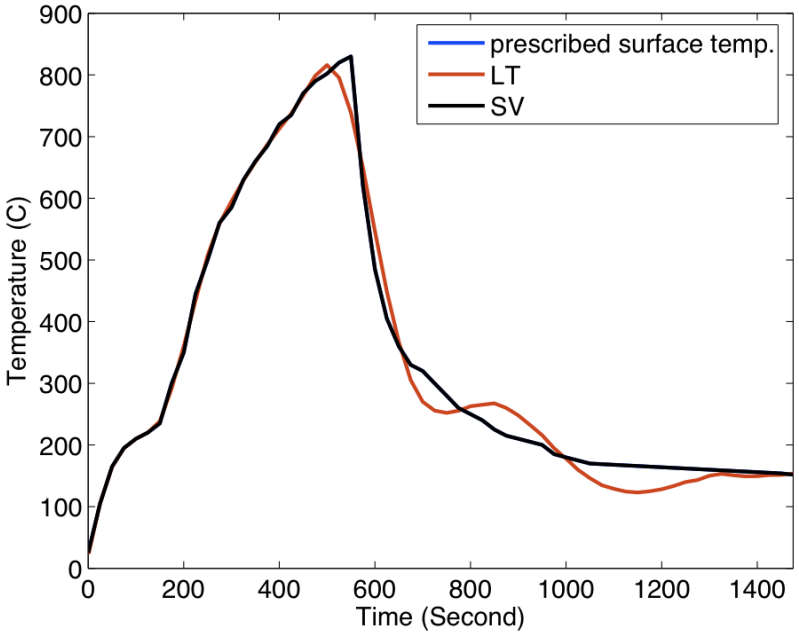

Figure 3.3: **Prescribed and Predicted Surface Temperatures at $r = 0$ for Different Times Based on LT and SV Methods**

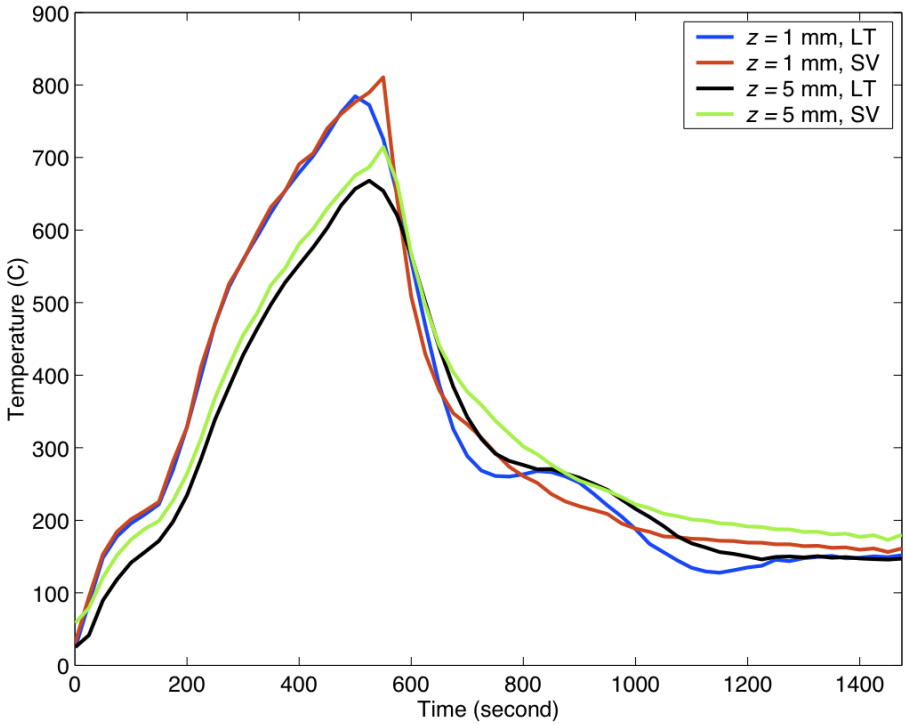

Figure 3.4: **Predicted Temperatures at $r = 0,\ z = 1$ mm and $r = 0,\ z = 5$ mm for Different Times**

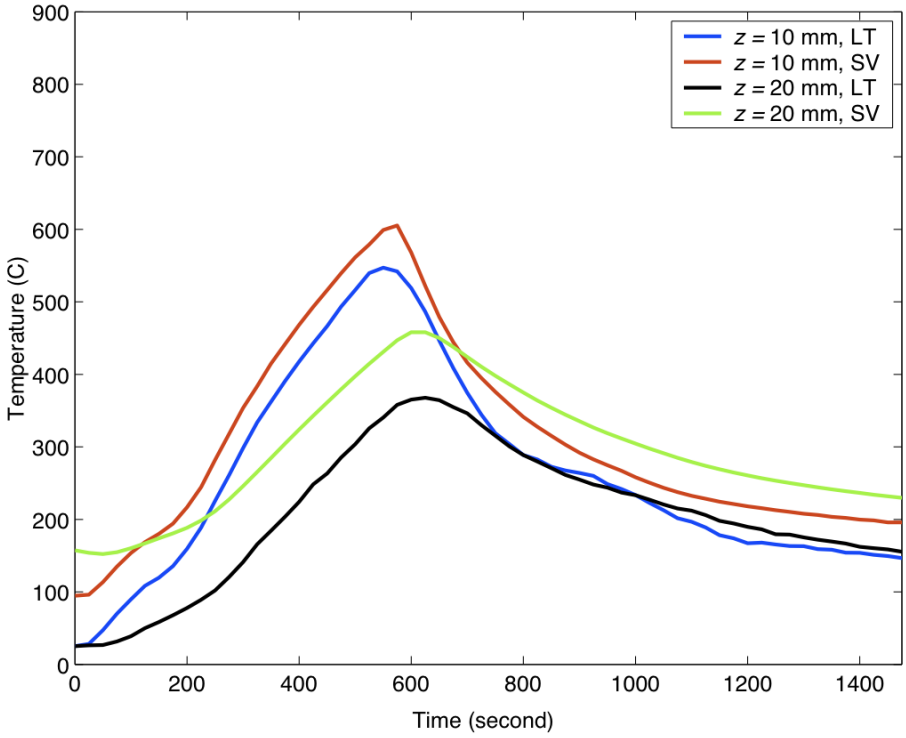

Figure 3.5: **Predicted Temperatures at $r = 0,\ z = 10$ mm and $r = 0,\ z = 20$ mm for Different Times**

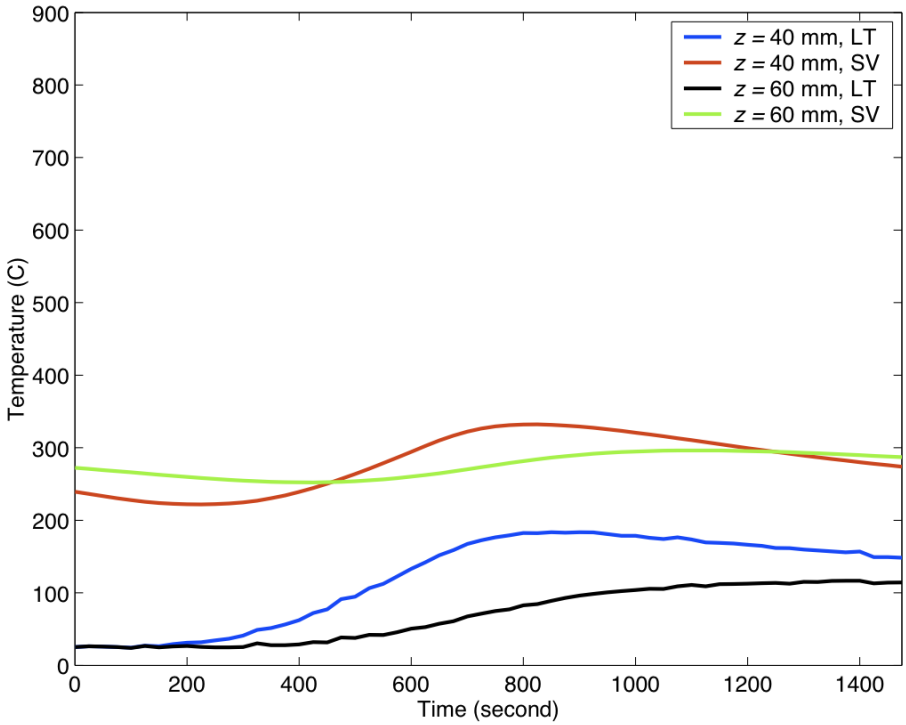

Figure 3.6: **Predicted Temperatures at $r = 0,\ z = 40$ mm and $r = 0,\ z = 60$ mm for Different Times**

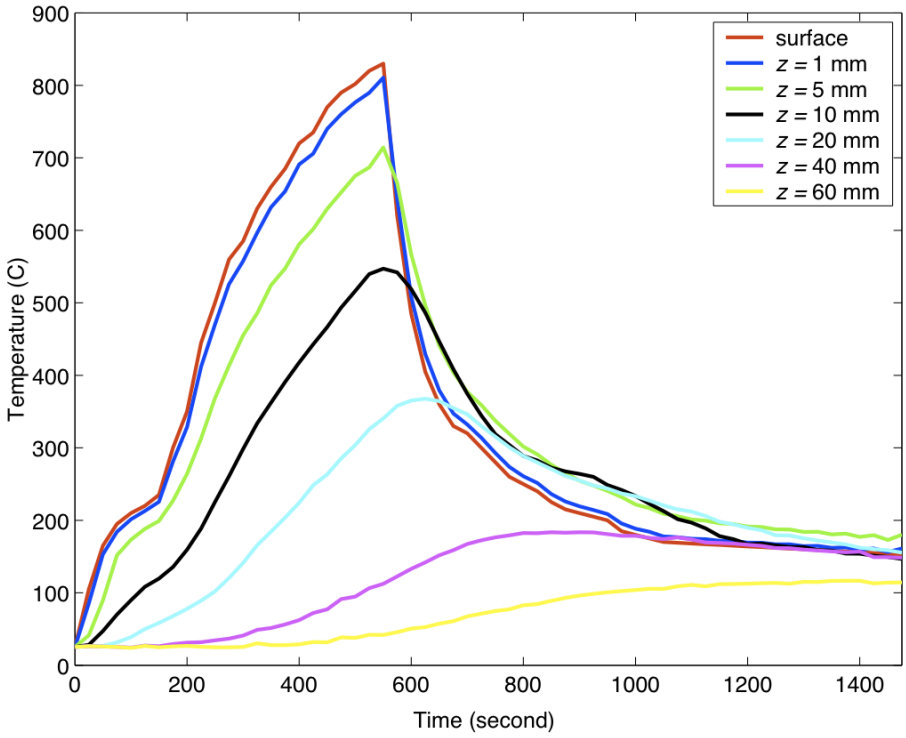

Figure 3.7: **Predicted Transient Temperatures at Different Depths Using Results Based on Two Methods Described in This Section**

Chapter 4

SUMMARY

This research work mainly concerns analytical solutions for predicting the rapidly varying temperature profile in pavements subjected to transient thermal loading. Analytical 1-D and axisymmetric 2-D solutions are developed in this technical report.

The general 1-D solution for a pavement temperature profile in homogeneous half-space with specified surface temperatures is well-known and can be resolved numerically using some powerful Gaussian-quadrature type integration formulas recommended in this report. Analytical solutions for the rapidly varying temperature profile in two-layered pavement systems are systematically investigated in this study and it is shown that they can be used to analyze the thermal effect of an innovative heat-resistant concrete layer overlying a conventional concrete base layer. The main mathematical tools employed in deriving temperature profiles in two-layered pavement systems are LT and numerical inversion of LT. One dimensional solutions are derived for input conditions both of specified surface temperature and of heat flux from aircraft engines. Model calculations suggest that the derived 1-D analytical solutions can capture the rapidly changing transient pavement temperature profile in both homogenous half-space and two-layered systems.

For the 2-D axisymmetric Dirichlet problem (i.e., pavement surface temperatures are known) in homogeneous half-space, specified axisymmetric transient surface temperatures are assumed and two solution methods are developed. The first method is based on HT and the method of SV, and the other is based on LT and HT. Numerical experiments suggest that a solution combining results generated by these two analytical methods can give reasonable predictions for actual rapidly varying temperature profiles.

References

[1] J. Ju and Y. Zhang, "A thermomechanical model for airfield concrete pavement under transient high temperature loadings," *International Journal of Damage Mechanics*, vol. 7, pp. 24–26, 1998.

[2] J. Ju and Y. Zhang, "Axisymmetric thermomechanical constitutive and damage modeling for airfield concrete pavement under transient high temperature," *Mechanics of Materials*, vol. 29, pp. 307–323, 1998.

[3] M. Hironaka and L. Malvar, "Av-8b aircraft exhaust blast resistant pavement systems," Tech. Rep. TR-2121-SHR, Naval Facilities Engineering Service Center, 2000.

[4] M. Hironaka and L. Malvar, "Jet exhaust damaged concrete," *Concrete International*, vol. 20, no. 10, pp. 32–35, 1998.

[5] M. Hironaka and L. Malvar, "F/a-18 apu resistant pavement systems," tech. rep., 1995.

[6] J. Roesler, "Theoretical solution for temperature profile in multi-layered pavement systems subjected to transient thermal loads." 2009.

[7] D. Wang, J. Roesler, and D.-Z. Guo, "An analytical approach to predicting temperature fields in multi-layered pavement systems," *Journal of Engineering Mechanics*, vol. 135, no. 4, pp. 334–344, 2009.

[8] Y. Zhang, *Thermo-micromechanical damage modeling for airfield concrete pavement*. PhD thesis, University of California, Los Angeles, 1997.

[9] W. Strauss, *Partial differential equations: an introduction*. John Wiley & Sons, Inc., 1992.

[10] H. Carslaw and J. C. Jaeger, *Conduction of Heat in Solids*. Oxford University Press, 1959.

[11] N. Steen, G. Byrne, and E. Gelbard, "Gaussian quadratures for the integrals $\int_0^\infty \exp(-x^2)f(x)dx$ and $\int_0^b \exp(-x^2)f(x)dx$," *Mathematics of Computation*, vol. 23, pp. 661–671, 1969.

[12] I. Sneddon, *The use of integral transforms*. McGraw-Hill Book Company, 1972.

[13] M. Spiegel, *Schaum's outline of theory and problems of Laplace transforms*. Schaum Publishing Co., 1965.

[14] P. Davis and P. Rabinowitz, *Methods of Numerical Integration*. Academic Press, Inc., 2nd ed., 1984.

[15] A. Stroud and D. Secrest, *Gaussian quadrature formulas*. Prentice-Hall, Inc., 1966.

[16] J. Davidovits, "Geopolymers: Inorganic polymeric new materials," *Journal of Thermal Analysis*, vol. 37, pp. 1633–1656, 1997.

[17] R. L. Burden and J. D. Faires, *Numerical Analysis*. Brooks/Cole, 7th ed., 2001.

[18] E. Zauderder, *Partial differential equations of applied mathematics*. John Wiley & Sons, Inc., 2006.

[19] R. Churchill, *Operational Mathematics*. McGraw-Hill Book Company, 3rd ed., 1972.

Appendix

This appendix lists the main Matlab and Fortran codes developed in this study.

1. 1-D Temperature Field in a Homogeneous Half-Space (Matlab codes)
    - homo_varied_z.m: calculate temperature profile at a fixed time t
    - homo_varied_t.m: calculate temperature history at a particular depth
2. 1-D Temperature Field in a Two-layered Pavement System (Matlab codes)
    (a) Specified Pavement Surface Temperatures
        - twolayer_varied_z.m: calculate temperature profile in the concrete layer at a fixed time t
        - twolayer_varied_t.m: calculate temperature history at a particular depth in the concrete layer
    (b) Mixed Boundary Conditions, i.e., Specified Heat Flux from Aircraft Engine
        - twolayer_mixed_bc_varied_z.m: calculate temperature profile in the concrete layer at a fixed time t
        - twolayer_mixed_bc_varied_t.m: calculate temperature history at a particular depth in the concrete layer
3. 2-D Axisymmetric Temperature Field in a Homogeneous Half-Space Subjected to Specified Pavement Surface Temperatures (Fortran source codes)
    (a) Separation of Variables Method
        - temphomo2.f: main code to calculate temperature history at a particular location in the concrete layer
        - gauss.f and w1.f: two subroutines

(b) Laplace Integral Transformation Method

- homolt.f: main code to calculate temperature history at a particular location in the concrete layer
- gauss.f and w1.f: two subroutines

LIST OF SYMBOLS AND ABBREVIATIONS

1-D	one-dimensional
2-D	two-dimensional
B	pavement surface convection coefficient (kcal/m^{2}hr °C)
BC	boundary condition(s)
F	function appeared in the boundary condition
G	function appeared in the initial condition
H_1	h_1
H_2	$h_1 + h_2$
HT	Hankel transform
$J_0(\xi r)$	first kind of Bessel function of order zero
LT	Laplace transform
$Q(t)$	heat flux emanating from the aircraft engines (kcal/m^2 h)
SV	separation of variables
T	temperature function (Celsius degree)
T_j	temperature function for layer j (Celsius degree)
$\bar{\hat{T}}(\xi, z, s)$	Laplace transformation of $T(r, z, t)$ with respect to t followed by Hankel transformation on r
U_j	shifted temperature function for layer j (Celsius degree)
$\hat{U}_j$	Laplace transformation of U_j
$Y(r, z, t)$	complex-valued function whose imaginary part is the desired temperature function
h_1	thickness of Portland cement concrete (m)
h_2	thickness of the base layer (m)
j, M, N	integers
r	radial variable (m)
s	Laplace transformation variable

t	temporal variable (s)
w_k	weights used in the Gaussian quadrature type formula
x_k	abscissae used in the Gaussian quadrature type formula
z	depths measured from pavement surface (m)
α	thermal diffusivity of material (m^2/h)
α_j	thermal diffusivity of the jth layer (m^2/h)
λ_j	thermal conductivity of the jth layer (kcal/m h °C)
μ	parameter to account for the temperature variation along the radial direction (1/m)
ξ	Hankel transformation variable
ϕ	phase angle (non-dimensional)
ω	frequency (1/hour)